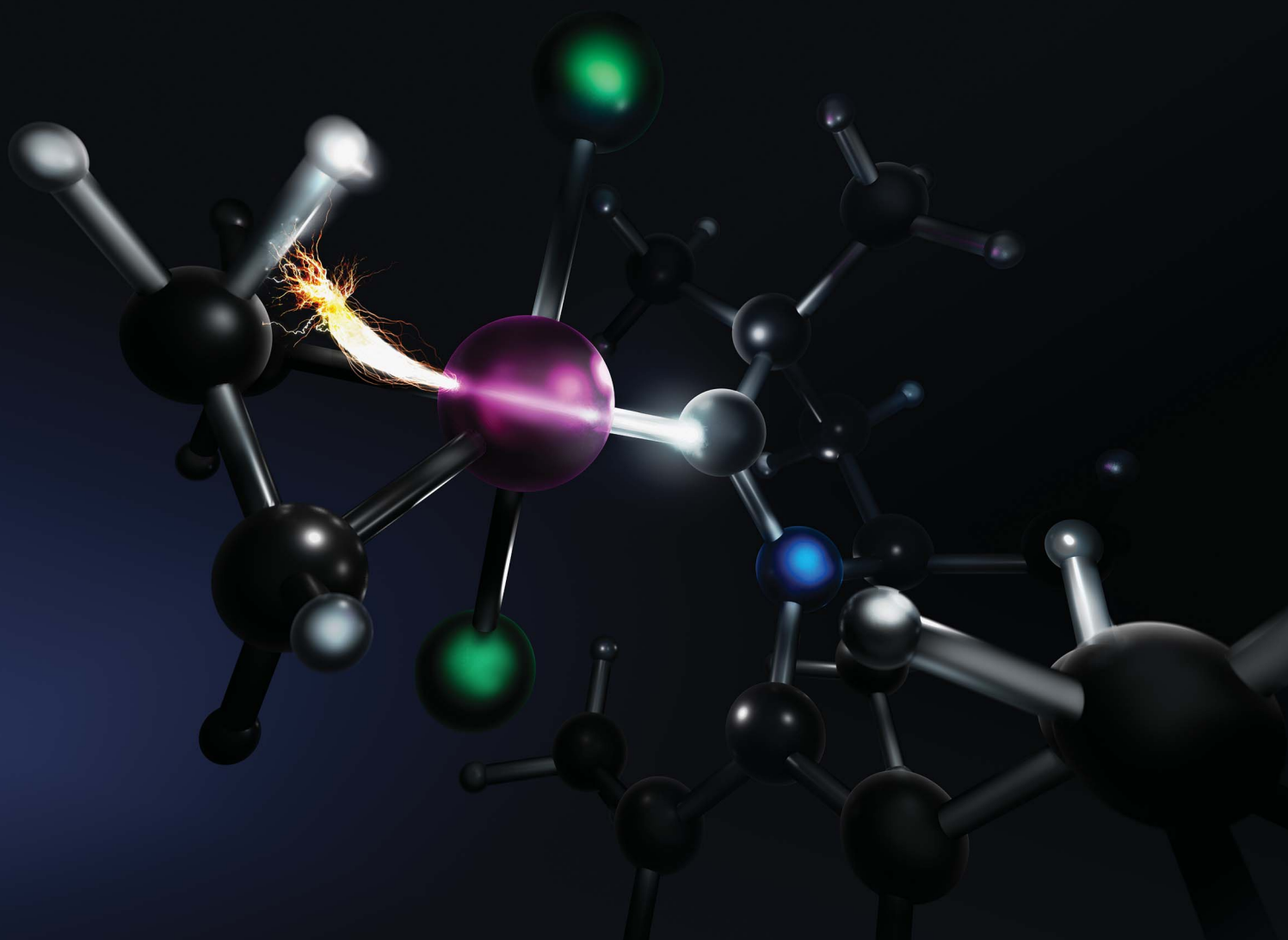


# Chemical Science

Volume 13  
Number 18  
14 May 2022  
Pages 5029–5418

[rsc.li/chemical-science](https://rsc.li/chemical-science)



ISSN 2041-6539

**EDGE ARTICLE**

Giovanni Occhipinti, Deryn E. Fogg, Vidar R. Jensen *et al.*  
The Janus face of high trans-effect carbenes in olefin  
metathesis: gateway to both productivity and decomposition

Cite this: *Chem. Sci.*, 2022, 13, 5107

All publication charges for this article have been paid for by the Royal Society of Chemistry

# The Janus face of high trans-effect carbenes in olefin metathesis: gateway to both productivity and decomposition†

Giovanni Occhipinti,<sup>a</sup> Daniel L. Nascimento,<sup>b</sup> Marco Foscato,<sup>a</sup> Deryn E. Fogg<sup>a,b</sup> and Vidar R. Jensen<sup>a</sup>

Ruthenium–cyclic(alkyl)(amino)carbene (CAAC) catalysts, used at ppm levels, can enable dramatically higher productivities in olefin metathesis than their N-heterocyclic carbene (NHC) predecessors. A key reason is the reduced susceptibility of the metallacyclobutane (MCB) intermediate to decomposition via  $\beta$ -H elimination. The factors responsible for promoting or inhibiting  $\beta$ -H elimination are explored via density functional theory (DFT) calculations, in metathesis of ethylene or styrene (a representative 1-olefin) by Ru–CAAC and Ru–NHC catalysts. Natural bond orbital analysis of the frontier orbitals confirms the greater strength of the orbital interactions for the CAAC species, and the consequent increase in the carbene trans influence and trans effect. The higher trans effect of the CAAC ligands inhibits  $\beta$ -H elimination by destabilizing the transition state (TS) for decomposition, in which an agostic MCB C $\beta$ –H bond is positioned trans to the carbene. Unproductive cycling with ethylene is also curbed, because ethylene is trans to the carbene ligand in the square pyramidal TS for ethylene metathesis. In contrast, metathesis of styrene proceeds via a ‘late’ TS with approximately trigonal bipyramidal geometry, in which carbene trans effects are reduced. Importantly, however, the positive impact of a strong trans-effect ligand in limiting  $\beta$ -H elimination is offset by its potent accelerating effect on bimolecular coupling, a major competing means of catalyst decomposition. These two decomposition pathways, known for decades to limit productivity in olefin metathesis, are revealed as distinct, antinomic, responses to a single underlying phenomenon. Reconciling these opposing effects emerges as a clear priority for design of robust, high-performing catalysts.

Received 10th February 2022  
Accepted 19th March 2022

DOI: 10.1039/d2sc00855f

rsc.li/chemical-science

## Introduction

Olefin metathesis is prized for its versatility in enabling the catalytic assembly of unactivated alkenes.<sup>1,2</sup> Long embraced in organic synthesis, metathesis methodologies are increasingly prominent in frontier applications in materials science<sup>3–19</sup> and chemical biology,<sup>20–22</sup> and in hybrid technologies such as DNA-encoded chemical libraries (DECL).<sup>23–25</sup> Recognized in these and a myriad of other applications (notably pharmaceutical manufacturing)<sup>26–29</sup> are challenges arising from catalyst decomposition. Indeed, despite a handful of examples in specialty-chemicals and pharmaceutical manufacturing,<sup>26</sup> industrial uptake of molecular olefin metathesis catalysts has

been much slower than anticipated when the ruthenium catalysts were first developed in the 1990s.<sup>30</sup>

Much effort has been committed to identifying the pathways that underlie decomposition of the widely-used ‘second-

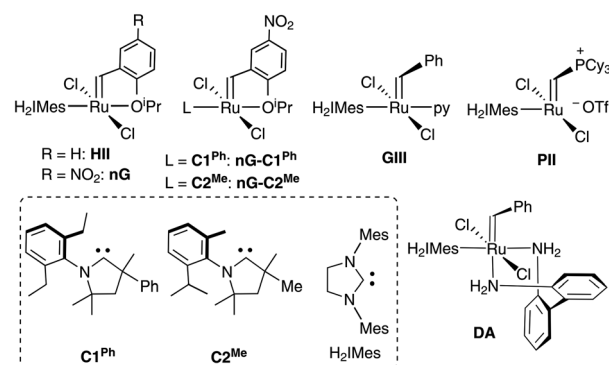


**Chart 1** Catalysts and carbene ligands discussed. The CAAC labelling system adopted<sup>42</sup> (C#<sup>R</sup>) numbers these ligands by common NAR moiety. The superscript R specifies the variable substituent on the quaternary site  $\alpha$  to the carbene carbon.

<sup>a</sup>Department of Chemistry, University of Bergen, Allégaten 41, N-5007 Bergen, Norway. E-mail: Giovanni.Occhipinti@uib.no; Deryn.Fogg@uib.no; Vidar.Jensen@uib.no

<sup>b</sup>Center for Catalysis Research & Innovation, Department of Chemistry and Biomolecular Sciences, University of Ottawa, Ottawa, Canada K1N 6N5. E-mail: dfogg@uottawa.ca

† Electronic supplementary information (ESI) available: Experimental and computational details, NMR spectra, and supplementary computational results and data (PDF). See DOI: 10.1039/d2sc00855f



generation" ruthenium catalysts<sup>31–33</sup> (in particular, the Hoveyda and nitro-Grela catalysts **HII** and **nG**; Chart 1, and their PCy<sub>3</sub>-stabilized predecessors, the Grubbs catalysts). Now well established are the mechanisms of degradation by nucleophiles<sup>34–37</sup> and Brønsted base.<sup>37,38</sup> As well, in advances critical for applications in chemical biology and related contexts (including DECL technology), we are beginning to understand how these catalysts decompose in water-rich environments.<sup>5,39–41</sup>

The dominant *intrinsic* decomposition modes – that is, pathways inherent to the catalysts themselves – involve bimolecular coupling of the [M]=CH<sub>2</sub> intermediates, and β-H elimination of the metallacyclobutane (MCB; Scheme 1).<sup>31–33</sup> We recently reported the first detailed mechanistic insights into the factors that govern bimolecular decomposition.<sup>42,43</sup> In contrast, the factors that cause β-H elimination of the MCB ring are not discussed even in comprehensive reviews,<sup>31–33</sup> despite the fact that this pathway has been recognized for decades for both d<sup>0</sup> catalysts<sup>44</sup> and the more robust Ru systems.<sup>45,46</sup>

In the broader context, the factors that promote or suppress β-H elimination for a given organometallic complex are incompletely resolved. Textbook requirements<sup>47</sup> are a vacant site cis to the alkyl ligand, and the capacity to adopt a *syn*-coplanar arrangement of the M–C<sub>α</sub>–C<sub>β</sub>–H moiety (but see below). Coordinative saturation and ligand bulk or rigidity can thus inhibit β-H elimination.<sup>47–50</sup> Recent studies reinforce the critical role of steric and geometric factors in enabling C–H agostic binding.<sup>49,51</sup> Aside from the requirement of an empty metal d orbital to accept electron density from the C<sub>β</sub>–H bond (the latter accounting for the known stability of d<sup>10</sup> metal alkyls),<sup>48,50</sup> electronic effects are less clear-cut.<sup>47–59</sup> Whereas a more electron-rich metal has been suggested to accelerate C<sub>β</sub>–H bond-breaking,<sup>54</sup> high trans-influence<sup>60</sup> ligands (typically strong donors, which increase electron density at the metal) have been reported to inhibit β-H elimination by destabilizing the required transition-state species.<sup>52,53,57–59</sup>

Insights into the parameters that govern β-H elimination have broad relevance in catalysis, given the central, enabling role of β-H elimination in certain contexts (*e.g.*, the Shell Higher Olefin Process,<sup>61</sup> Mizoroki–Heck coupling),<sup>62,63</sup> and its detrimental role in others (*e.g.*, olefin polymerization,<sup>64</sup> Suzuki–Miyaura coupling,<sup>65</sup> ring-closing or cross-metathesis (RCM, CM) of terminal olefins). Critical in the latter two reactions is formation of an unsubstituted MCB that is particularly

susceptible to β-H elimination.<sup>66</sup> This vulnerability underlies the highly detrimental impact of ethylene on metathesis by Ru–NHC and Ru–phosphine catalysts,<sup>67</sup> documented in process chemistry,<sup>26–29</sup> continuous-flow metathesis,<sup>68–72</sup> and in the renewables sector,<sup>26,73,74</sup> where CM with ethylene ('ethenolysis') would otherwise offer the simplest, most powerful means of transforming fatty acid methyl esters (FAMES) into α-olefins. Less discussed, but likewise critical, are the implications for stereoselective olefin metathesis, given the ability of isomerization-active catalyst decomposition products to erode the selectivity designed into the precatalysts.<sup>75–77</sup>

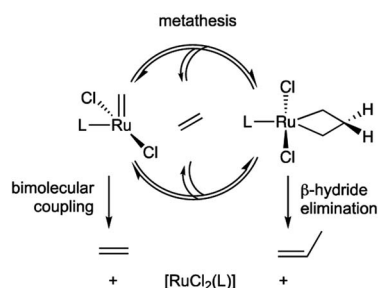
Until very recently, the ethylene-sensitivity of the ruthenium catalysts, and their susceptibility to decomposition *via* β-H elimination, have resisted solution. Because the latter reaction is unimolecular, it cannot be addressed by catalyst immobilization or use of high-dilution conditions. A lack of consensus on the factors responsible has hampered efforts to achieve highly productive Ru catalysts *via* rational catalyst redesign. The experimental finding that Ru–CAAC catalysts resist β-H elimination,<sup>78</sup> unlike their first- and second-generation Ru–phosphine and Ru–NHC predecessors, is thus important. In practical terms, this stability contributes to the unprecedented productivity reported for CAAC catalysts at ppm loadings in RCM macrocyclization,<sup>79,80</sup> ethenolysis of FAMES,<sup>80–82</sup> and acrylonitrile CM.<sup>79</sup> More fundamentally, it offers new opportunities to clarify the factors that promote or inhibit β-H elimination.

Clarifying these factors is the main objective of the present work. To that end, we compare Ru–NHC and Ru–CAAC catalysts for which the susceptibility or resistance to β-H elimination, respectively, are established experimentally. We demonstrate that the high trans effect of the CAAC ligand, a consequence of the strength of the Ru–CAAC bond, is responsible for suppressing this decomposition pathway. The capacity of a high trans-effect ligand to inhibit β-H elimination indeed merits much broader recognition than it has received to date. In the context of olefin metathesis, this labilizing effect holds added importance: it is known to have a further, deleterious impact, accelerating decomposition *via* bimolecular coupling of [M]=CH<sub>2</sub> intermediates. These two decomposition pathways, known for decades to limit productivity in olefin metathesis, are thus seen for the first time to be related: they are opposing responses to the strong trans effect arising from strong metal-carbene binding.

## Results and discussion

### Assessing the proportion of β-H elimination vs. bimolecular coupling

In a prior experimental study, we demonstrated that decomposition of the CAAC catalysts **nG-C1<sup>Ph</sup>** and **nG-C2<sup>Me</sup>** occurs almost solely *via* bimolecular coupling (BMC).<sup>78</sup> Contrasting behavior was observed for H<sub>2</sub>IMes catalysts (**HII**, **nG**, **PII**, **DA**, **GIII**), all of which decomposed *via* a combination of BMC and β-H elimination, with the exception of **GIII**.<sup>43</sup> Diagnostic for β-H elimination is the observation of propene products, formed *via* loss of the metallacyclobutane ring. While the yield of propenes for **nG-C1<sup>Ph</sup>** or **nG-C2<sup>Me</sup>** was nearly nil, it was >50% for, *e.g.*, the



Scheme 1 Decomposition of intermediates in Ru-catalyzed olefin metathesis *via* bimolecular coupling or β-H elimination.



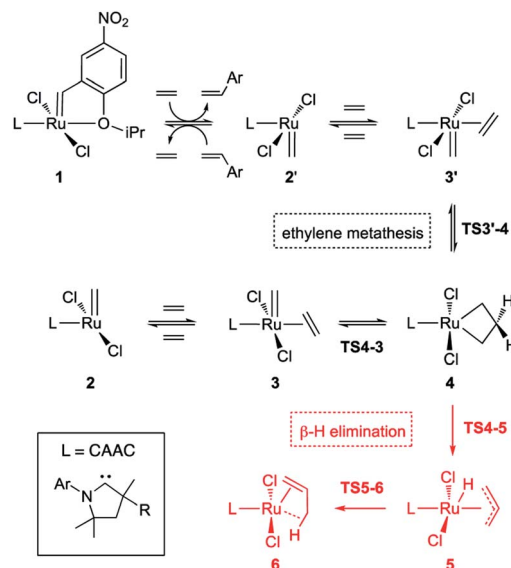
widely-used Grela catalyst **nG** (Fig. 1a). The H<sub>2</sub>IMes systems clearly decompose *via* competing unimolecular and bimolecular pathways.

Importantly, however, our original experiments were conducted at ruthenium concentrations of 20 mM, to achieve acceptable signal-to-noise levels in the NMR spectra of the catalysts and their propene decomposition products. To probe whether  $\beta$ -H elimination may be masked by rapid bimolecular decomposition under these conditions, we repeated these experiments with **nG-C1<sup>Ph</sup>** and **nG** at 1 mM Ru, using a higher NMR field strength to improve resolution and sensitivity. The proportion of  $\beta$ -H elimination was essentially unaffected for **nG-C1<sup>Ph</sup>** (3% over 72 h; Fig. 1b). For **nG**, it increased sharply, to 95%. We infer that the CAAC catalyst is indeed largely immune to this unimolecular decomposition pathway, whereas for **nG**, decomposition is dominated by  $\beta$ -H elimination at catalyst concentrations of 1 mM or below.

Unexpectedly, sustained liberation of propenes was observed in the **nG** experiment over 72 h, although no signals for the precatalyst could be observed after 24 h. We attribute the discrepancy to the continued presence of the metal-lacyclobutane complex, which goes undetected at RT owing to the breadth of its NMR signals (an indicator of fluxionality or exchange). In assessing complete catalyst decomposition, the intensity of the NMR signals for the organic products is evidently of greater quantitative value than those for the Ru species.

### Density functional theory (DFT) studies of ethylene-triggered decomposition

In studies of H<sub>2</sub>IMes complexes, the unsubstituted MCB has been identified as much more susceptible to  $\beta$ -H elimination than its substituted analogues.<sup>66</sup> In the present calculations, we therefore focused on the unsubstituted MCB. Scheme 2 depicts the  $\beta$ -H elimination and ethylene self-metathesis pathways examined. In these metathesis reactions, the position of the alkylidene 'flips' in every cycle. Methylidene complex 2', for



**Scheme 2** Ethylene self-metathesis and  $\beta$ -H elimination of MCB **4** ( $L = \text{H}_2\text{IMes}$ , **C1<sup>Ph</sup>**, **C2<sup>Me</sup>**). The prime symbol refers to rotamers of the CAAC complexes in which the quaternary CMe<sub>2</sub> or CMePh site  $\alpha$  to the carbene carbon is *syn* to the methylidene. Discussion of the stability and reactivity of the Ru-CAAC rotamers is deferred to a later stage.

example, could be viewed as a rotamer of **2**, generated by rotation of the ligand about the Ru-L bond. Carbene rotation, however, has an energetic price. The barriers *via* TS2'-2 are 22.8 or 30.6 kcal mol<sup>-1</sup> for **C1<sup>Ph</sup>** and **C2<sup>Me</sup>**, respectively (Table S2<sup>†</sup>), 3.3 or 11.3 kcal higher than the corresponding barriers to ethylene metathesis. Even less likely is carbene rotation in the ethylene complexes, which, with a barrier of 42.7 kcal mol<sup>-1</sup> *via* TS3'-3 for **C2<sup>Me</sup>**, appears prohibitive. Metathesis is thus the preferred mode of exchange between 2/3 and 2'/3' species.

This has important implications for the CAAC complexes, owing to their lack of symmetry. In all three square-pyramidal precatalysts **1**, the most stable geometry is that in which the alkylidene and the CAAC NAr group are *syn*-disposed (see subsection "The CAAC-Ru rotamers" below). Reaction with ethylene generates the active 14-electron complex 2', in which the methylidene is anti to the CAAC NAr moiety. Reaction of 2' with ethylene affords the square-pyramidal  $\pi$ -complex 3', in which the bound ethylene and the methylidene ligand are mutually perpendicular. Cycloaddition generates the trigonal bipyramidal (TBP) MCB intermediate **4**, which upon cycloreversion gives  $\pi$ -complex 3. The latter releases ethylene to form the most stable 14-electron methylidene complex **2**, thus completing the unproductive ethylene metathesis reaction. The reverse pathway starts from **2** and ends with 2'.

In the absence of competing reactions, this process is repeated until MCB **4** decomposes *via*  $\beta$ -H elimination (Scheme 2, pathway in red; Fig. 2).<sup>83</sup> The latter reaction involves Ru insertion into the  $\beta$ -C-H bond of the MCB to form allyl-hydride complex **5**, followed by hydride transfer to the terminal carbon of the allyl ligand to give  $\pi$ -complex **6**, which can then dissociate propene. When a non-isomerizable olefin is used (*e.g.*, ethylene

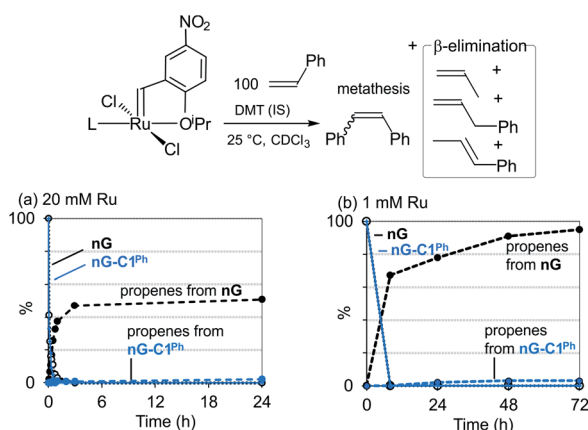


**Fig. 1** Decomposition of **nG** and **nG-C1<sup>Ph</sup>** *via*  $\beta$ -H elimination: disappearance of NMR signals for  $[\text{Ru}] = \text{CHAr}$ , and appearance of signals for propenes. (a) At 20 mM Ru (300 MHz). (b) At 1 mM Ru (500 MHz).

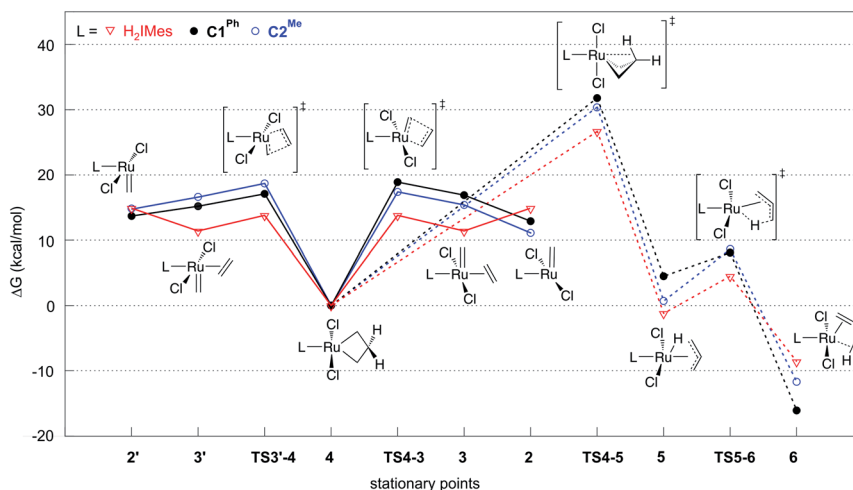


Fig. 2 Gibbs free energies of intermediates and transition states in ethylene self-metathesis (solid lines) and  $\beta$ -H elimination (dashed lines). Energies are relative to metallacyclobutane **4**, the resting state in ethylene self-metathesis. The individual elementary reactions are given in Scheme 2.

or styrene), propenes are a clear and unambiguous marker for decomposition *via*  $\beta$ -H elimination.<sup>42,43,78</sup>

Reaction of the catalyst precursors with ethylene to form the unsubstituted MCB **4** is exergonic in all cases (by 3.3–5.7 kcal mol<sup>−1</sup>; see Table S2†). Intermediate **4** is the on-cycle resting state. It is also the starting point for catalyst decomposition *via*  $\beta$ -H elimination, and hence the reference point against which free energies are calculated (Fig. 2, Table S2†).  $\beta$ -H elimination to form allyl hydride **5** from **4** *via* **TS4-5** (dashed lines, Fig. 2) involves a higher activation barrier for CAAC catalysts **nG-C1<sup>Ph</sup>** or **nG-C2<sup>Me</sup>** than **H<sub>2</sub>IMes** catalyst **nG** (by 5.1 or 3.7 kcal mol<sup>−1</sup>, respectively). These DFT-calculated differences in free-energy barriers are sufficiently large that less  $\beta$ -H elimination is expected for CAAC catalysts than for **nG**, consistent with the much higher proportion of propene decomposition products for the latter.<sup>78</sup>

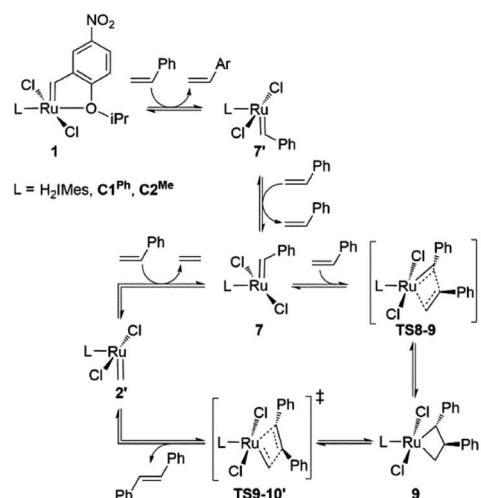
It may be noted that  $\beta$ -H elimination for any of these MCBs is expected to be slower than for any corresponding acyclic structures, because the requirement for *syn*-coplanarity<sup>47</sup> noted in the Introduction cannot be met.  $\beta$ -H elimination necessitates a compromise between the required *syn*-coplanar Ru-C $\alpha$ -C $\beta$ -H $\beta$  structure, and the energetically preferred planarity of the MCB ring in **4**. Puckering of the MCB ring (the Ru-C $\alpha$ -C $\beta$ -C $\alpha$  dihedral angle is in the range 53–56° in **TS4-5**) enables a reduction in the Ru-C $\alpha$ -C $\beta$ -H $\beta$  dihedral angle by more than 70° on going from **4** (where it is *ca.* 119°) to **TS4-5**.

Importantly, the calculations also predict that the **H<sub>2</sub>IMes** catalyst will react with ethylene more readily than do its CAAC counterparts. Whereas ethylene binding to methylidene complexes **2/2'** to form  $\pi$ -complexes **3/3'** is endergonic for the CAAC catalysts, ethylene binding stabilizes the **H<sub>2</sub>IMes** catalyst; it also lowers the barrier to MCB formation *via* **TS4-3** or **TS3'-4**. We will return to the origin of this difference below. Although somewhat slower MCB formation is predicted for the CAAC catalysts, the barriers to formation of **4** from **2/2'** are negligible. More significantly, the preferred Ru methylidene rotamer **2** is

2.0–3.8 kcal mol<sup>−1</sup> more stable (*vs.* the resting state **4**) for the CAAC complexes than their **H<sub>2</sub>IMes** analogue. Higher concentrations of the 14-electron methylidene **2** will therefore be present during catalysis for the CAAC catalysts, accounting for their faster decomposition *via* bimolecular coupling.<sup>42,43</sup>

### Decomposition during 1-alkene metathesis

Slower  $\beta$ -H elimination is one clear contributor to the heightened metathesis productivity of the CAAC metallacyclobutane **4**, relative to the **H<sub>2</sub>IMes** derivative. Here we evaluate the relative metathesis productivity of these catalysts, by comparing their barriers to  $\beta$ -H elimination (*via* **TS4-5**) *vs.* those to self-metathesis of styrene to form trans-stilbene (Scheme 3, Fig. 3). The barriers to metathesis are determined by the



Scheme 3 Key intermediates and transition states for styrene self-metathesis. For clarity, only the energetically most favored catalytic cycles, commencing with the 14-electron benzylidene species **7** and ending with 14-electron methylidene species **2'**, are depicted.<sup>84</sup>





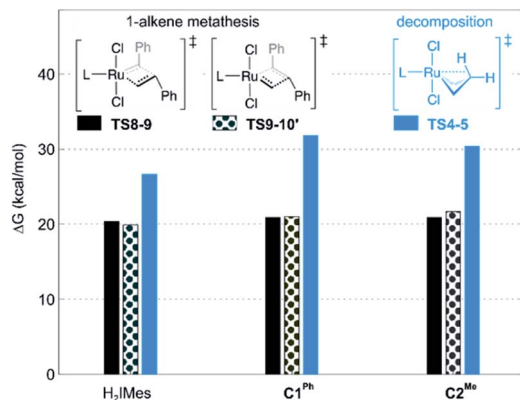


Fig. 3 Barriers to 1-alkene metathesis (via TS8-9 and TS9-10') or  $\beta$ -H elimination (via TS4-5). Free energies are given relative to the unsubstituted metallacyclobutane 4.

transition state for cycloaddition (TS8-9) or retro-addition (TS9-10'). The symmetry of the H<sub>2</sub>IMes ligand results in a single reaction pathway each for metathesis and  $\beta$ -H elimination. For the unsymmetrical CAAC complexes, four competing pathways are operative for each of these reactions (see the ESI† for details). The two energetically favored pathways (corresponding to Pathways 3 and 4 in Table S2†) involve cycloaddition transition states TS8-9, with the benzylidene-derived phenyl moiety *syn* to the NAr group. These rotamers imply a catalytic cycle commencing with 14-electron benzylidene species 7 and ending with 14-electron methylidene species 2', as depicted in Scheme 3. In the preferred, lowest-barrier pathway, the benzylidene moiety is oriented away from the quaternary phenyl substituent of C1<sup>Ph</sup>, or the isopropyl substituent of C2<sup>Me</sup>. The corresponding transition state for retro-addition is TS9-10', in which the methylidene moiety is *syn* to the quaternary site.

A smaller energy difference between the barriers to  $\beta$ -H elimination (TS4-5 vs. 4) and styrene metathesis (TS8-9 or TS9-10' vs. 4, whichever is the less stable) is seen for the H<sub>2</sub>IMes catalyst than the CAAC catalysts. Specifically, the difference is 6.3 kcal mol<sup>-1</sup> for nG, vs. 10.4 or 8.7 kcal mol<sup>-1</sup>, respectively, for nG-C1<sup>Ph</sup> or nG-C2<sup>Me</sup>; see Fig. 3. The H<sub>2</sub>IMes catalyst thus has a lower energetic 'buffer' against  $\beta$ -H elimination from the unsubstituted MCB, consistent with its greater susceptibility to this decomposition pathway.<sup>78</sup>

All catalysts studied exhibited a higher barrier to styrene self-metathesis than ethylene metathesis, presumably resulting from both the steric bulk<sup>85</sup> and the electron-withdrawing properties of the phenyl substituent.<sup>86</sup> For the H<sub>2</sub>IMes catalyst nG, the difference is 6.6 kcal mol<sup>-1</sup>, vs. 2.6 or 3.1 kcal mol<sup>-1</sup> for nG-C1<sup>Ph</sup> or nG-C2<sup>Me</sup>, respectively. This reinforces the more facile reaction of nG with ethylene discussed above. The CAAC catalysts are thus predicted to have a greater bias toward 1-alkene metathesis. Their lower reactivity toward ethylene is expected to increase productivity at high 1-alkene conversions, by limiting unproductive cycling with the ethylene co-product of metathesis, which opens the door to decomposition of the unsubstituted MCB. Conversely, at low conversions, 1-alkene coupling should be faster with the H<sub>2</sub>IMes catalyst, which has

the lowest calculated barrier to styrene self-metathesis. This is consistent with the observed bias of NHC catalysts toward self-metathesis at low conversions in ethenolysis experiments.<sup>74</sup>

### Factors determining the rates of metathesis and $\beta$ -H elimination

To probe the stereoelectronic factors responsible for the outstanding productivity and robustness of the CAAC catalysts, we examined properties of the carbene ligands and their Ru complexes. In general, CAAC ligands are known to have less stable  $\sigma$ -donor orbitals and more stable  $\pi$ -acceptor orbitals than corresponding cyclic diaminocarbenes, and therefore to be both better  $\sigma$ -donors and  $\pi$ -acceptors.<sup>87–92</sup> To obtain a first, qualitative comparison of the donor/acceptor properties specific to the three leading carbenes under study, we calculated the energies of their frontier orbitals, focusing on those with the shape and symmetry appropriate for bonding interactions with the metal (Fig. 4).<sup>93,94</sup> Carbene  $\sigma$ -donation is dominated by the highest-energy occupied molecular orbital (HOMO), which is centered on the carbene carbon atom and has  $\sigma$ -symmetry with respect to the metal–carbene bond. The lowest unoccupied carbene frontier orbital with  $\pi$ -symmetry. The energies of the frontier orbitals suggest that the two CAAC ligands should have similar donor/acceptor properties, but that both should be better  $\sigma$ -donors and better  $\pi$ -acceptors than H<sub>2</sub>IMes.

Critical in metathesis is the impact of these differences on the frontier orbital energies in the unsubstituted MCB. Following the procedure described in ref. 95, natural bond orbital (NBO) analysis<sup>96</sup> of 4 confirmed stronger  $\sigma$ -donation as well as  $\pi$ -back-donation for the CAAC complexes (donation/back-donation = 0.66/0.20 and 0.67/0.21 electrons for C1<sup>Ph</sup> and C2<sup>Me</sup>, respectively) than for the H<sub>2</sub>IMes complex (0.57/0.15 electrons). The stronger orbital interactions for the CAAC ligands give rise to stronger bonds to ruthenium: the calculated bond dissociation free energies are *ca.* 5 kcal mol<sup>-1</sup> higher (42.8 and 43.3 kcal mol<sup>-1</sup> for C1<sup>Ph</sup> and C2<sup>Me</sup>, respectively) than for H<sub>2</sub>IMes (38.0 kcal mol<sup>-1</sup>).

Importantly, the stronger metal–carbene orbital interactions result in a higher trans influence and trans effect for the CAAC ligands.<sup>60</sup> In addition to weakening trans-positioned bonds in equilibrium geometries, the strong orbital interactions of the CAAC ligands have critical kinetic consequences. In transition

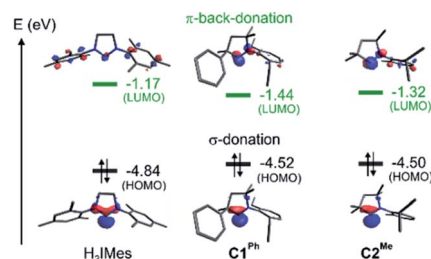


Fig. 4 Energies and shapes, given as isosurface plots of  $\pm \phi(x,y,z) = 0.08$  a.u., of the DFT (Kohn–Sham) frontier orbitals most relevant to the carbene  $\sigma$ -donor and  $\pi$ -acceptor properties.



state **TS4-5**, the rupturing C<sub>β</sub>-H bond approaches the ruthenium center trans to the carbene (Fig. 5a and 6a). It thus necessitates mutual trans interactions of two high trans-effect ligands, the carbene and the nascent hydride. This is more costly for a CAAC than a H<sub>2</sub>IMes MCB. The higher barrier to β-H elimination for the former is thus proposed to arise from the higher trans effect characteristic of the CAAC carbenes, relative to H<sub>2</sub>IMes.

The proposed role of the trans effect is confirmed by an NBO-based second-order perturbation analysis of donor-acceptor interactions in **TS4-5** (Fig. 6; Table 1). The carbene lone pair and the β-C-H bond compete for σ-donation to the same Ru acceptor orbital. Simultaneously, the carbene π-acceptor orbital and the antibonding β-C-H and Ru-C orbitals compete for the same Ru lone pair. That is, the increased competition for donation and back-donation at the transition state retards β-H elimination for the CAAC complexes.

Computational studies of alkyl cross-coupling *via* group 10 catalysts describe similar retarding effects where β-H elimination occurs trans to dative ligands of strong trans effect.<sup>52,53</sup> Likewise, high trans-effect anionic ligands (X) have been found to retard oxidative addition of methane and ammonia at the site trans to X in Ir(I) complexes.<sup>97</sup> A related, more indirect, effect on the rate of β-H elimination has been observed in olefin metathesis for d<sup>0</sup> molybdenum and tungsten catalysts, in which higher barriers to β-H elimination have been calculated for oxo-stabilized MCBs than for their imido analogues.<sup>58</sup> The d<sup>0</sup> metal catalysts preferentially undergo β-H elimination after isomerizing to a square-pyramidal MCB, in which the C<sub>β</sub>-H bond approaches the metal cis, rather than trans, to the imido or oxo ligand. The latter ligands are trans to one of the rupturing M-C

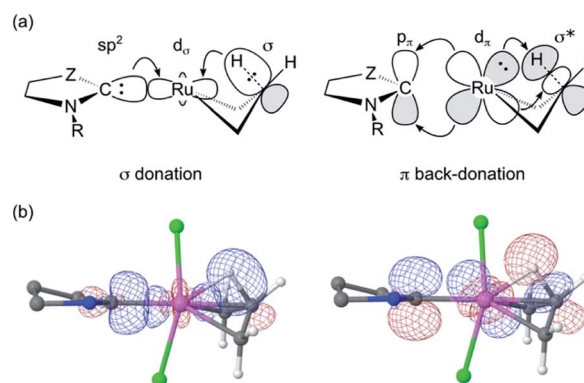


Fig. 6 (a) Idealized representation of competing molecular orbital interactions affecting the energy of **TS4-5** (see Table 1 for donor-acceptor interaction energies). For clarity, only the most relevant atoms are shown. Z = NAr or CRR'. (b) Combined isosurface representations (cutoff = 0.09 a.u.) of the three natural bond orbitals involved in the competition for σ-donation (left) and π-back-donation (right) in **TS4-5** for **C1<sup>Ph</sup>**. Ru: pink; Cl: green; C: grey; N: blue; H: white. Hydrogen atoms and substituents of **C1<sup>Ph</sup>** have been omitted for clarity.

bonds of the MCB, and hence destabilize the β-H elimination transition state<sup>58</sup> (particularly the oxo ligand, which has a stronger trans effect).<sup>60</sup> A similar role of the oxo ligand in retarding β-H elimination was recently described for vanadium-oxo olefin metathesis catalysts.<sup>57</sup> Taken together, all these examples suggest that high trans-effect ligands offer an important general strategy, valid across multiple catalytic manifolds, to suppress β-H elimination.

In ruthenium-catalyzed olefin metathesis, the capacity of the high trans-effect carbene ligand to inhibit β-H elimination can now be explicitly identified as a key contributor to the remarkable productivity of the CAAC catalysts. The high trans effect also has negative consequences, however, as we recently demonstrated: the labilizing effect of the CAAC ligand increases the concentration of the four-coordinate methylidene species **2/2'**, and thus promotes decomposition *via* bimolecular coupling.<sup>42</sup> These two decomposition pathways, long viewed as independent, can now be recognized as opposing responses to a single underlying phenomenon, which originates in strong ligand binding. This is particularly important given the transformative role played by strong carbene donicity in Ru-catalyzed olefin metathesis.<sup>30,98</sup>

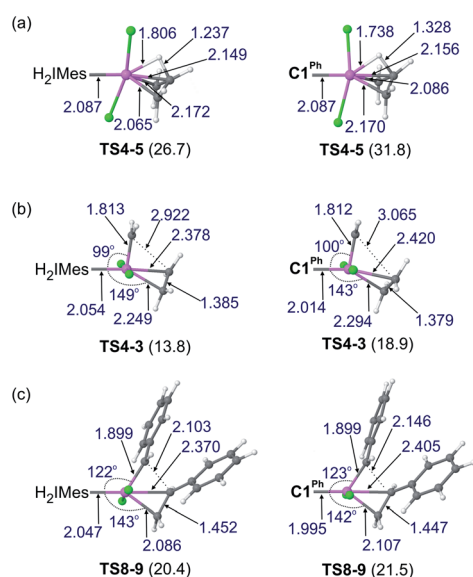


Fig. 5 Optimized geometries for transition-state species corresponding to key barriers for: (a) β-H elimination; (b) ethylene self-metathesis; (c) styrene self-metathesis. Ru: pink; Cl: green; C: grey; H: white. Shown are selected bond distances (Å), bond angles (°), and (in parentheses) the Gibbs free energy (kcal/mol; in CHCl<sub>3</sub>) relative to **4**, the most stable reaction intermediate.

Table 1 Donor-acceptor interaction energies of NBO-based second-order perturbation analysis of **TS4-5**

Carbene	Donor-acceptor interaction energy <sup>a</sup> (kcal mol <sup>-1</sup> )			
	sp <sup>2</sup> → d <sub>σ</sub>	σ → d <sub>σ</sub>	d <sub>π</sub> → p <sub>π</sub>	d <sub>π</sub> → σ*
H <sub>2</sub> IMes	141.3	50.4	37.8	6.9
<b>C1<sup>Ph</sup></b>	143.2	61.9	19.6	7.6
<b>C2<sup>Me</sup></b>	135.2	63.7	17.3	10.0

<sup>a</sup> The orbital labels are defined in Fig. 6.

In addition to retarding  $\beta$ -H elimination, the high trans influence of the CAAC ligands destabilizes the ethylene  $\pi$ -complexes **3/3'**, in which ethylene (also a high trans-influence ligand) binds trans to the carbene. "Early" transition states are seen en route to the MCB **4** (**TS3'-4** and **TS4-3**). That is, the TS geometries closely resemble those of the square-pyramidal  $\pi$ -complexes (Fig. 5b): the ethylene ligand is still far from parallel to the Ru=CH<sub>2</sub> bond,<sup>99–101</sup> and the double bond is nearly intact, with very little interaction with the methylidene, as suggested by a Wiberg bond index (WBI, a bond-order measure)<sup>102</sup> of >1.5 for the ethylene C <sub>$\alpha$</sub> –C <sub>$\beta$</sub>  bond, and <0.15 for its C <sub>$\beta$</sub> –C <sub>$\alpha$</sub>  bond to the methylidene (see Fig. S8†). In consequence, the trans influence that affects the ethylene  $\pi$ -complexes is also manifested in a trans effect. The latter kinetic effect retards ethylene self-metathesis by destabilizing the early,  $\pi$ -complex-like transition states (behavior analogous to that seen in  $\beta$ -H elimination *via* **TS4-5** above). The barrier to metathesis of ethylene hence increases by *ca.* 5 kcal mol<sup>–1</sup> for the CAAC complexes, compared to the H<sub>2</sub>IMes analogue.

Styrene self-metathesis, in contrast, is found to proceed *via* a "late" transition state (*e.g.*, **TS8-9**, Fig. 5c). The geometry of the latter resembles that of the MCB intermediate **4**: it shows a significantly elongated styrene double bond (1.45 Å, compared to 1.35 Å in free styrene), and clear interaction with the benzylic carbon, with a C–C distance only slightly longer than 2 Å. Ruthenacyclobutane intermediates, and transition states (such as **TS8-9**) that resemble such intermediates, have distorted TBP geometries. The MCB ring lies in the trigonal plane, and no ligand is bound trans to the carbene, unlike the  $\pi$ -complexes **3/3'** and the early transition states **TS3'-4** and **TS4-3**. Within the trigonal plane, strong bonds exist between the Ru center, the carbene ligand, and the MCB C <sub>$\alpha$</sub>  atoms. Positioned trans to the carbene, but with a Ru–C <sub>$\beta$</sub>  distance 0.28–0.51 Å longer than the Ru–C <sub>$\alpha$</sub>  bonds, is the  $\beta$ -carbon atom. The latter interacts weakly with Ru, unsurprisingly given that it already engages in four  $\sigma$ -bonds (MCB intermediates) or is well on the way to forming the fourth  $\sigma$ -bond (**TS8-9** and **TS9-10'**). The Ru–C <sub>$\beta$</sub>  Wiberg bond indices of these late transition states (0.11–0.14; see Fig. S8†) are a small fraction of those calculated for the strong metal–ligand bonds in the trigonal plane, and only *ca.* half those of Ru–C <sub>$\beta$</sub>  bonds of the early transition states **TS3'-4** and **TS4-3**.

Styrene metathesis is thus little affected by the carbene trans effect, in contrast to  $\beta$ -H elimination and ethylene self-metathesis. Indeed, the barriers to styrene metathesis are within 1.3 kcal mol<sup>–1</sup> for all three catalysts. All are higher than the barriers to ethylene self-metathesis, as noted above, but the energetic preference for ethylene self-metathesis is higher for the H<sub>2</sub>IMes catalyst than its CAAC analogues (by 6.6, 2.1 or 3.0 kcal mol<sup>–1</sup> for **nG**, **nG-C1<sup>Ph</sup>** and **nG-C2<sup>Me</sup>**, respectively); see Fig. 7.

These differences in barrier heights imply that the CAAC catalysts are less susceptible to non-productive cycling with ethylene. The superior productivity of the CAAC catalysts thus arises not merely from their resistance to  $\beta$ -H elimination, but from their improved selectivity for 1-alkenes, relative to ethylene. The slightly reduced preference for ethylene self-metathesis calculated for **nG-C1<sup>Ph</sup>**, *vs.* **nG-C2<sup>Me</sup>** (a difference

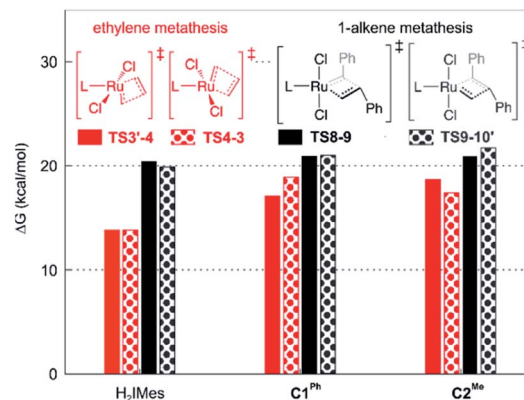


Fig. 7 Calculated barriers to metathesis of ethylene *vs.* styrene (in kcal mol<sup>–1</sup>, *vs.* **4**).

of 0.9 kcal mol<sup>–1</sup>) is presumed to reinforce the positive effects of the quaternary phenyl substituent on metathesis productivity.<sup>79,103</sup>

Again, the favorable properties of the CAAC ligands originate in the high trans effect exerted by these carbenes in the transition states for  $\beta$ -H elimination and ethylene self-metathesis.

In contrast, and perhaps surprisingly, steric differences between the three carbenes do not seem to play a significant role. Their overall steric features are similar, as judged from both the buried volumes<sup>104</sup> calculated for **4** (%V<sub>bur</sub> = 33.6%, 36.2%, and 34.3% for H<sub>2</sub>IMes, C1<sup>Ph</sup>, and C2<sup>Me</sup>, respectively) and the natural steric exchange repulsion energy<sup>105</sup> calculated between the carbene, the methylidene, and the chloride ligands in the methylidene complexes **2/2'** (28.8/28.8 kcal mol<sup>–1</sup>, 33.0/35.1 kcal mol<sup>–1</sup>, and 30.9/28.8 kcal mol<sup>–1</sup>, for H<sub>2</sub>IMes, C1<sup>Ph</sup>, and C2<sup>Me</sup>, respectively; see the ESI for details). From both methods, C1<sup>Ph</sup> appears only slightly bulkier than H<sub>2</sub>IMes and C2<sup>Me</sup>. In short, neither the differences in overall bulk, nor those in spatial steric distribution (as represented by steric maps;<sup>104</sup> see the ESI†), appear sufficient to account for the robustness and productivity of the two CAAC catalysts.

### The CAAC–Ru rotamers

As a final point, the relative stability and reactivities of the various rotamers – an inevitable complication arising from the asymmetry of the CAAC ligands – deserves some comment. Within the C2<sup>Me</sup> catalyst system, rotamer **2** (in which the methylidene ligand is anti to the quaternary site flanking the carbene carbon) is more stable than rotamer **2'** by 3.7 kcal mol (see Fig. 2), despite the lower steric exchange repulsion (by 2.1 kcal mol<sup>–1</sup>) calculated for the latter. The explanation lies in overriding electronic effects (Fig. 8). Whereas **2'** is destabilized by strong electrostatic repulsion between the methylidene and the nearby quaternary methyl groups, **2** is stabilized by attraction between the quaternary methyl groups and the chloride ligands. Similar, but weaker, attractive interactions between the chloride ligands and the NAr alkyl groups stabilize **2'**. In **2**, the electrostatic repulsion between the NAr alkyl groups and the methylidene is much weaker than the corresponding repulsion



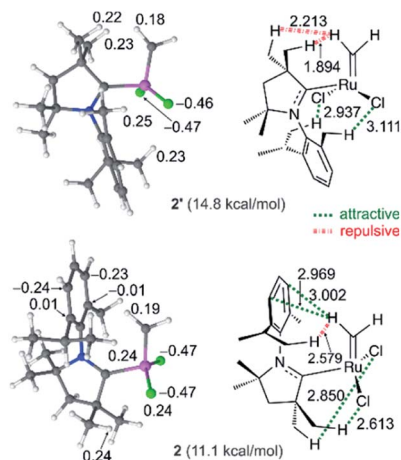


Fig. 8 Natural charges (e) of selected atoms appear in the ball-and-stick models of the optimized geometries (left). Repulsive and attractive interactions, and selected atomic distances (Å), of rotamers 2/2' of nG-C2<sup>Me</sup> (right). Ru: pink; Cl: green; C: grey; N: blue; H: white. Given in parentheses are the free energies vs. 4.

from the quaternary methyl groups in 2' and is also offset by stabilizing polar CH- $\pi$  interactions<sup>42,106</sup> between the methylidene and the aromatic NAr group. The calculations thus predict that in the most stable geometry 2, the NAr group is *syn* to the alkylidene. In fact, within the C2<sup>Me</sup> catalyst system, this rotamer was found to be preferred for all the alkylidene species and ethylene self-metathesis transition states studied.  $\pi$ -Face donation from the C<sub>ipso</sub> atom of the NAr to the alkylidene carbon atom<sup>107–109</sup> is also expected to stabilize the *syn* conformation of alkylidenes parallel to the NAr plane, such as in the ethylene complex 3, and in corresponding transition state TS4-3.

In contrast, the aromatic quaternary substituent of nG-C1<sup>Ph</sup> engages in attractive polar CH- $\pi$  interactions<sup>42,106</sup> with the alkylidene, stabilizing those rotamers in which the quaternary CAAC site is *syn* to the alkylidene. The latter represent the most stable ethylene complex (3') and corresponding transition state (TS3'-4) leading to 4. Consistent with these contrasting predicted rotamer stabilities, NOESY-NMR analysis revealed interactions between the [Ru]=CHAr proton and the quaternary phenyl group for the Piers-class catalyst P-C1<sup>Ph</sup> (Chart 1; Fig. S4†), but not for P-C2<sup>Me</sup>. Likewise, [Ru]=CH<sub>2</sub>-phenyl interactions could be detected for a pyridine-stabilized derivative of 2' for C1<sup>Ph</sup>, although rapid decomposition precluded unambiguous interpretation of the spectrum for the C2<sup>Me</sup> analogue.

This phenyl-induced stabilization of a rotamer that is destabilized in nG-C2<sup>Me</sup> facilitates metathesis by nG-C1<sup>Ph</sup>. Facile alkylidene 'flipping' promotes engagement of both rotamers in catalysis, and their relative stability has a positive impact on the transition states connecting them to the rest of the catalytic cycle. For example, the barrier to styrene self-metathesis for nG-C1<sup>Ph</sup> is lower by 0.7 kcal mol<sup>-1</sup> compared to nG-C2<sup>Me</sup>, thereby further improving the selectivity for 1-alkene vs. ethylene metathesis.

## Conclusions

Unlike their NHC predecessors (notably those bearing an H<sub>2</sub>Imes ligand), the ruthenium-CAAC metathesis catalysts studied are essentially immune to decomposition *via*  $\beta$ -H elimination from the metallacyclobutane. Calculations predict a higher barrier to  $\beta$ -H elimination in the CAAC systems, consistent with the distinctions in behavior observed experimentally. Also predicted is higher selectivity for metathesis of styrene, vs. unproductive ethylene self-metathesis, relative to the Ru-NHC catalysts. The poorer selectivity of the latter (that is, their tendency to engage in metathesis of ethylene), in conjunction with the greater vulnerability to  $\beta$ -H elimination of the unsubstituted MCB thus formed, represent a lethal combination of effects that explains the lower metathesis productivity of the popular NHC catalysts relative to the emerging CAAC systems.

The higher barriers to  $\beta$ -H elimination and ethylene self-metathesis calculated for the CAAC catalysts originate in the stronger carbene-metal orbital interactions. These interactions destabilize both intermediates (trans influence) and transition states (trans effect) involving competing orbital interactions trans to the carbene, notably TS4-5 ( $\beta$ -H elimination) and TS3'-4/TS4-3 (ethylene self-metathesis). Thus, both the greater resistance to  $\beta$ -H elimination and the improved selectivity for productive 1-alkene metathesis of the CAAC catalysts are due to the higher trans effect of this carbene class.

The findings above add ruthenium olefin metathesis catalysts to the systems for which high trans-influence ligands have been found to retard  $\beta$ -H elimination,<sup>52,53,57,58</sup> underlining the generality and the scope of this ligand effect in catalysis. Crucially, for ruthenium, the impact is manifested in lower rates of reaction (both  $\beta$ -H elimination and ethylene cycloaddition) taking place directly trans to the ligand.

The high trans influence and trans effect are clearly critical to the breakthrough success of the CAAC ligand family. However, these properties also have a profound negative consequence, greatly enhancing the susceptibility to bimolecular coupling of 4-coordinate methylidene species 2/2'.<sup>42</sup> The positive impact of a strong trans-effect ligand in limiting  $\beta$ -H elimination is thus offset by its potent accelerating effect on bimolecular decomposition. These two decomposition pathways have long been known to limit productivity in olefin metathesis. They are here revealed as distinct, antinomic, responses to a single underlying phenomenon. Reconciling these opposing effects is a clear priority for catalyst design. More robust and productive olefin metathesis catalysts will aid in expanding applications in demanding contexts. One specific, compelling goal is the development of stereoselective catalysts resistant to  $\beta$ -H elimination, including as-yet-undiscovered stereoselective CAAC catalysts.

## Data availability

The complete computational data is available from the ioChem-BD repository,<sup>110</sup> *via* <https://doi.org/10.19061/iochem-bd-6-113>.



## Author contributions

DEF and VRJ designed and supervised the project. GO performed the DFT calculations, with initial contributions from MF. MF handled, organized, and stored the computational data (see Data availability). DLN performed the experiments. All authors analyzed the computational and experimental results. GO wrote the initial draft. DEF and VRJ wrote the final manuscript, with contributions from GO, MF, and DLN. All authors have approved the final manuscript.

## Conflicts of interest

There are no conflicts to declare.

## Acknowledgements

This work was funded by the Natural Sciences and Engineering Research Council of Canada (NSERC) and by the Research Council of Norway (RCN, via Projects 262370, 288135, 226244, NN2506K, and NS2506K). The Government of Ontario is thanked for an International Ontario Graduate Scholarship to DLN.

## Notes and references

- 1 *Handbook of Metathesis*, ed. R. H. Grubbs, A. G. Wenzel, D. J. O'Leary and E. Khosravi, Wiley-VCH, Weinheim, 2nd edn, 2015.
- 2 *Olefin Metathesis: Theory and Practice*, ed. K. Grela, John Wiley & Sons, Inc., Hoboken, NJ, 2014.
- 3 A. Rizzo, G. I. Peterson, A. Bhaumik, C. Kang and T.-L. Choi, *Angew. Chem., Int. Ed.*, 2021, **60**, 849–855.
- 4 T. Debsharma, B. Schmidt, A. Laschewsky and H. Schlaad, *Macromolecules*, 2021, **54**, 2720–2728.
- 5 J. C. Foster, M. C. Grocott, L. A. Arkinstall, S. Varlas, M. J. Redding, S. M. Grayson and R. K. O'Reilly, *J. Am. Chem. Soc.*, 2020, **142**, 13878–13885.
- 6 D. C. Church, L. Takiguchi and J. K. Pokorski, *Polym. Chem.*, 2020, **11**, 4492–4499.
- 7 J. D. Feist and Y. Xia, *J. Am. Chem. Soc.*, 2020, **142**, 1186–1189.
- 8 S. Varlas, J. C. Foster and R. K. O'Reilly, *Chem. Commun.*, 2019, **55**, 9066–9071.
- 9 S. Varlas, R. Keogh, Y. Xie, S. L. Horswell, J. C. Foster and R. K. O'Reilly, *J. Am. Chem. Soc.*, 2019, **141**, 20234–20248.
- 10 T. Debsharma, F. N. Behrendt, A. Laschewsky and H. Schlaad, *Angew. Chem., Int. Ed.*, 2019, **58**, 6718–6721.
- 11 K. Jung, T. S. Ahmed, J. Lee, J.-C. Sung, H. Keum, R. H. Grubbs and T.-L. Choi, *Chem. Sci.*, 2019, **10**, 8955–8963.
- 12 K. Song, K. Kim, D. Hong, J. Kim, C. E. Heo, H. I. Kim and S. H. Hong, *Nat. Commun.*, 2019, **10**, 3860.
- 13 J. P. Edwards, W. J. Wolf and R. H. Grubbs, *J. Polym. Sci., Part A: Polym. Chem.*, 2019, **57**, 228–242.
- 14 C. Theunissen, M. A. Ashley and T. Rovis, *J. Am. Chem. Soc.*, 2019, **141**, 6791–6796.
- 15 P. Liu and C. Ai, *Ind. Eng. Chem. Res.*, 2018, **57**, 3807–3820.
- 16 Y. Dong, J. B. Matson and K. J. Edgar, *Biomacromolecules*, 2017, **18**, 1661–1676.
- 17 A.-C. Knall and C. Slugovc, in *Olefin Metathesis: Theory and Practice*, ed. K. Grela, John Wiley & Sons, Inc., Hoboken, NJ, 2014, pp. 269–284.
- 18 E.-H. Kang, S. Y. Yu, I. S. Lee, S. E. Park and T.-L. Choi, *J. Am. Chem. Soc.*, 2014, **136**, 10508–10514.
- 19 K. Merrett, W. Liu, D. Mitra, K. D. Camm, C. R. McLaughlin, Y. Liu, M. A. Watsky, F. Li, M. Griffith and D. E. Fogg, *Biomaterials*, 2009, **30**, 5403–5408.
- 20 M. S. Messina and H. D. Maynard, *Mater. Chem. Front.*, 2020, **4**, 1040–1051.
- 21 P. G. Isenegger and B. G. Davis, *J. Am. Chem. Soc.*, 2019, **141**, 8005–8013.
- 22 E. V. Vinogradova, *Pure Appl. Chem.*, 2017, **89**, 1619–1640.
- 23 O. B. C. Monty, P. Nyshadham, K. M. Bohren, M. Palaniappan, M. M. Matzuk, D. W. Young and N. Simmons, *ACS Comb. Sci.*, 2020, **22**, 80–88.
- 24 O. B. C. Monty, N. Simmons, S. Chamakuri, M. M. Matzuk and D. W. Young, *ACS Comb. Sci.*, 2020, **22**, 833–843.
- 25 X. Lu, L. Fan, C. B. Phelps, C. P. Davie and C. P. Donahue, *Bioconjug. Chem.*, 2017, **28**, 1625–1629.
- 26 C. S. Higman, J. A. M. Lummiss and D. E. Fogg, *Angew. Chem., Int. Ed.*, 2016, **55**, 3552–3565.
- 27 M. Yu, S. Lou and F. Gonzalez-Bobes, *Org. Process Res. Dev.*, 2018, **22**, 918–946.
- 28 V. Farina and A. Horváth, in *Handbook of Metathesis*, ed. R. H. Grubbs, A. G. Wenzel, D. J. O'Leary and E. Khosravi, Wiley-VCH, Weinheim, 2nd edn, 2015, vol. 2, pp. 633–658.
- 29 K. R. Fandrick, J. Savoie, N. Yee, J. J. Song and C. H. Senanayake, in *Olefin Metathesis: Theory and Practice*, ed. K. Grela, John Wiley & Sons, Inc., 2014, pp. 349–365.
- 30 T. M. Trnka and R. H. Grubbs, *Acc. Chem. Res.*, 2001, **34**, 18–29.
- 31 M. Jawiczuk, A. Marczyk and B. Trzaskowski, *Catalysts*, 2020, **10**, 887–942.
- 32 Y. Schrodli, in *Handbook of Metathesis*, ed. R. H. Grubbs, A. G. Wenzel, D. J. O'Leary and E. Khosravi, Wiley-VCH, Weinheim, 2015, vol. 1, pp. 323–342.
- 33 J. C. Chadwick, R. Duchateau, Z. Freixa and P. W. N. M. van Leeuwen, in *Homogeneous Catalysts: Activity – Stability – Deactivation*, Wiley-VCH, Weinheim, 1st edn, 2011, pp. 347–396.
- 34 W. L. McClennan, S. A. Rufh, J. A. Lummiss and D. E. Fogg, *J. Am. Chem. Soc.*, 2016, **138**, 14668–14677.
- 35 J. A. M. Lummiss, W. L. McClennan, R. McDonald and D. E. Fogg, *Organometallics*, 2014, **33**, 6738–6741.
- 36 S. H. Hong, A. G. Wenzel, T. T. Salguero, M. W. Day and R. H. Grubbs, *J. Am. Chem. Soc.*, 2007, **129**, 7961–7968.
- 37 B. J. Ireland, B. T. Dobigny and D. E. Fogg, *ACS Catal.*, 2015, **5**, 4690–4698.
- 38 G. A. Bailey, J. A. M. Lummiss, M. Foscatto, G. Occhipinti, R. McDonald, V. R. Jensen and D. E. Fogg, *J. Am. Chem. Soc.*, 2017, **139**, 16446–16449.



- 39 A. Y. Goudreault, D. M. Walden, D. L. Nascimento, A. G. Botti, S. N. Steinmann, C. Michel and D. E. Fogg, *ACS Catal.*, 2020, **10**, 3838–3843.
- 40 C. O. Blanco, J. Sims, D. L. Nascimento, A. Y. Goudreault, S. N. Steinmann, C. Michel and D. E. Fogg, *ACS Catal.*, 2021, **11**, 893–899.
- 41 T. Matsuo, T. Yoshida, A. Fujii, K. Kawahara and S. Hirota, *Organometallics*, 2013, **32**, 5313–5319.
- 42 D. L. Nascimento, M. Foscato, G. Occhipinti, V. R. Jensen and D. E. Fogg, *J. Am. Chem. Soc.*, 2021, **143**, 11072–11079.
- 43 G. A. Bailey, M. Foscato, C. S. Higman, C. S. Day, V. R. Jensen and D. E. Fogg, *J. Am. Chem. Soc.*, 2018, **140**, 6931–6944.
- 44 R. R. Schrock, J. S. Murdzek, G. C. Bazan, J. Robbins, M. DiMare and M. O'Regan, *J. Am. Chem. Soc.*, 1990, **112**, 3875–3886.
- 45 W. Janse van Rensburg, P. J. Steynberg, W. H. Meyer, M. M. Kirk and G. S. Forman, *J. Am. Chem. Soc.*, 2004, **126**, 14332–14333.
- 46 P. E. Romero and W. E. Piers, *J. Am. Chem. Soc.*, 2007, **129**, 1698–1704.
- 47 J. F. Hartwig, in *Organotransition Metal Chemistry: From Bonding to Catalysis*, University Science Books, Mill Valley, CA, USA, 2010, *ch. 10*, pp. 398–406.
- 48 M. Castiñeira Reis, C. S. López, E. Kraka, D. Cremer and O. N. Faza, *Inorg. Chem.*, 2016, **55**, 8636–8645.
- 49 S. M. Bellows, T. R. Cundari and P. L. Holland, *Organometallics*, 2013, **32**, 4741–4751.
- 50 G. Klatt, R. Xu, M. Pernpointner, L. Molinari, T. Quang Hung, F. Rominger, A. S. K. Hashmi and H. Köppel, *Chem.–Eur. J.*, 2013, **19**, 3954–3961.
- 51 T. Debnath, T. Ash, T. Banu and A. K. Das, *Theor. Chem. Acc.*, 2016, **135**, 175.
- 52 B. Pudasaini and B. G. Janesko, *Organometallics*, 2014, **33**, 84–93.
- 53 B. Pudasaini and B. G. Janesko, *Organometallics*, 2012, **31**, 4610–4618.
- 54 D. Tanaka, S. P. Romeril and A. G. Myers, *J. Am. Chem. Soc.*, 2005, **127**, 10323–10333.
- 55 J. F. Hartwig, S. Richards, D. Barañano and F. Paul, *J. Am. Chem. Soc.*, 1996, **118**, 3626–3633.
- 56 X. Solans-Monfort, C. Coperet and O. Eisenstein, *J. Am. Chem. Soc.*, 2010, **132**, 7750–7757.
- 57 D. S. Belov, D. A. Fenoll, I. Chakraborty, X. Solans-Monfort and K. V. Bukhryakov, *Organometallics*, 2021, **40**, 2939–2944.
- 58 X. Solans-Monfort, C. Copéret and O. Eisenstein, *Organometallics*, 2012, **31**, 6812–6822.
- 59 N. Koga, S. Obara, K. Kitaura and K. Morokuma, *J. Am. Chem. Soc.*, 1985, **107**, 7109–7116.
- 60 The literature discussions center on *trans* influence, a thermodynamic parameter. In our own analysis in the discussion that follows, we emphasize (with some exceptions) the role of the *trans* effect, as this controls the kinetics of catalyst decomposition.
- 61 W. Keim, *Angew. Chem., Int. Ed.*, 2013, **52**, 12492–12496.
- 62 T. Mizoroki, K. Mori and A. Ozaki, *Bull. Chem. Soc. Jpn.*, 1971, **44**, 581.
- 63 R. F. Heck and J. P. Nolley, *J. Org. Chem.*, 1972, **37**, 2320–2322.
- 64 C. Chen, *Nat. Rev. Chem.*, 2018, **2**, 6–14.
- 65 I. P. Beletskaya, F. Alonso and V. Tyurin, *Coord. Chem. Rev.*, 2019, **385**, 137–173.
- 66 J. Engel, W. Smit, M. Foscato, G. Occhipinti, K. W. Törnroos and V. R. Jensen, *J. Am. Chem. Soc.*, 2017, **139**, 16609–16619.
- 67 A. H. Hoveyda, Z. Liu, C. Qin, T. Koengeter and Y. Mu, *Angew. Chem., Int. Ed.*, 2020, **59**, 22324–22348.
- 68 J. Morvan, T. McBride, I. Curbet, S. Colombel-Rouen, T. Roisnel, C. Crévisy, D. L. Browne and M. Mauduit, *Angew. Chem., Int. Ed.*, 2021, **60**, 19685–19690.
- 69 C. P. Breen, C. Parrish, N. Shangguan, S. Majumdar, H. Murnen, T. F. Jamison and M. M. Bio, *Org. Process Res. Dev.*, 2020, **24**, 2298–2303.
- 70 K. Skowerski, S. J. Czarnocki and P. Knapkiewicz, *ChemSusChem*, 2014, **7**, 536–542.
- 71 S. Monfette, M. Eyholzer, D. M. Roberge and D. E. Fogg, *Chem.–Eur. J.*, 2010, **16**, 11720–11725.
- 72 Z. Lysenko, B. R. Maughon, T. Mokhtar-Zadeh and M. L. Tulchinsky, *J. Organomet. Chem.*, 2006, **691**, 5197–5203.
- 73 J. Spekrijse, J. P. M. Sanders, J. H. Bitter and E. L. Scott, *ChemSusChem*, 2017, **10**, 470–482.
- 74 R. Kadyrov, C. Azap, S. Weidlich and D. Wolf, *Top. Catal.*, 2012, **55**, 538–542.
- 75 T. P. Montgomery, A. M. Johns and R. H. Grubbs, *Catalysts*, 2017, **7**, 87.
- 76 M. B. Herbert, B. A. Suslick, P. Liu, L. Zou, P. K. Dornan, K. N. Houk and R. H. Grubbs, *Organometallics*, 2015, **34**, 2858–2869.
- 77 G. Occhipinti, F. R. Hansen, K. W. Törnroos and V. R. Jensen, *J. Am. Chem. Soc.*, 2013, **135**, 3331–3334.
- 78 D. L. Nascimento and D. E. Fogg, *J. Am. Chem. Soc.*, 2019, **141**, 19236–19240.
- 79 R. Gawin, A. Tracz, M. Chwalba, A. Kozakiewicz, B. Trzaskowski and K. Skowerski, *ACS Catal.*, 2017, **7**, 5443–5449.
- 80 D. L. Nascimento, A. Gawin, R. Gawin, P. A. Guńka, J. Zachara, K. Skowerski and D. E. Fogg, *J. Am. Chem. Soc.*, 2019, **141**, 10626–10631.
- 81 A. Kajetanowicz, M. Chwalba, A. Gawin, A. Tracz and K. Grela, *Eur. J. Lipid Sci. Technol.*, 2020, **122**, 1900263.
- 82 V. M. Marx, A. H. Sullivan, M. Melaimi, S. C. Virgil, B. K. Keitz, D. S. Weinberger, G. Bertrand and R. H. Grubbs, *Angew. Chem., Int. Ed.*, 2015, **54**, 1919–1923.
- 83 Whereas the metathesis-active MCB intermediates of d<sup>0</sup> tungsten and molybdenum catalysts isomerize from a distorted TBP structure to a square-based pyramidal structure (SP) before decomposing *via* β-H-elimination, the corresponding TBP–SP isomerization for ruthenium catalysts with realistic, bulky ligands such as H<sub>2</sub>IMes involves high free-energy barriers (>30 kcal mol<sup>−1</sup> for H<sub>2</sub>IMes) that effectively prevent such isomerization; see



- P. R. Remya and C. H. Suresh, *J. Comput. Chem.*, 2017, **38**, 1704–1711.
- 84 The prime symbol indicates the rotamer in which the quaternary site  $\alpha$  to the carbene carbon (*i.e.*, CMe<sub>2</sub> or CMePh) is *syn* to the alkylidene. Thus, in **TS8-9**, the benzylidene moiety is located *syn* to the NAr group. In the preferred, lowest-barrier pathway, the benzylidene phenyl substituent in **TS8-9** is oriented away from the quaternary phenyl or isopropyl substituents for C1<sup>Ph</sup> and C2<sup>Me</sup>, respectively.
- 85 S. Fomine, J. V. Ortega and M. A. Tlenkopatchev, *J. Organomet. Chem.*, 2006, **691**, 3343–3348.
- 86 P. Tobón, S. Gómez, A. Restrepo and F. Núñez-Zarur, *Organometallics*, 2021, **40**, 119–133.
- 87 C. A. Gaggioli, G. Bistoni, G. Ciancaleoni, F. Tarantelli, L. Belpassi and P. Belanzoni, *Chem.–Eur. J.*, 2017, **23**, 7558–7569.
- 88 U. S. D. Paul and U. Radius, *Eur. J. Inorg. Chem.*, 2017, 3362–3375.
- 89 M. Melaimi, R. Jazzar, M. Soleilhavoup and G. Bertrand, *Angew. Chem., Int. Ed.*, 2017, **56**, 10046–10068.
- 90 U. S. D. Paul, C. Sieck, M. Haehnel, K. Hammond, T. B. Marder and U. Radius, *Chem.–Eur. J.*, 2016, **22**, 11005–11014.
- 91 K. C. Mondal, S. Roy, B. Maity, D. Koley and H. W. Roesky, *Inorg. Chem.*, 2016, **55**, 163–169.
- 92 A. A. Tukov, A. T. Normand and M. S. Nechaev, *Dalton Trans.*, 2009, 7015–7028.
- 93 D. P. Chong, O. V. Gritsenko and E. J. Baerends, *J. Chem. Phys.*, 2002, **116**, 1760–1772.
- 94 R. Stowasser and R. Hoffmann, *J. Am. Chem. Soc.*, 1999, **121**, 3414–3420.
- 95 NBO analyses were performed on the geometry optimized intermediate **4** and on the carbene fragment “frozen” in the geometry of complex **4**, respectively. The difference in electron population between the ylidene carbon lone pair of the isolated carbene fragment and that of the  $\sigma$ -symmetric Ru–L natural bonding orbital in **4** was taken as a measure of  $\sigma$ -donation. The corresponding difference in electron population between the ylidene carbon lone vacancy in the carbene fragment and in **4** was taken as a measure of  $\pi$ -back-donation. To ensure that population differences were calculated for identical Lewis structures, the latter were explicitly defined *via* the NBO \$CHOOSE input section. See the ESI† for details.
- 96 E. D. Glendening, C. R. Landis and F. Weinhold, *J. Comput. Chem.*, 2013, **34**, 1429–1437.
- 97 D. Y. Wang, Y. Choliy, M. C. Haibach, J. F. Hartwig, K. Krogh-Jespersen and A. S. Goldman, *J. Am. Chem. Soc.*, 2016, **138**, 149–163.
- 98 G. Occhipinti, H.-R. Bjørsvik and V. R. Jensen, *J. Am. Chem. Soc.*, 2006, **128**, 6952–6964.
- 99 W. Smit, M. Foscato, G. Occhipinti and V. R. Jensen, *ACS Catal.*, 2020, **10**, 6788–6797.
- 100 C. E. Webster, *J. Am. Chem. Soc.*, 2007, **129**, 7490–7491.
- 101 C. Adlhart and P. Chen, *J. Am. Chem. Soc.*, 2004, **126**, 3496–3510.
- 102 K. B. Wiberg, *Tetrahedron*, 1968, **24**, 1083–1096.
- 103 D. L. Nascimento, I. Reim, M. Foscato, V. R. Jensen and D. E. Fogg, *ACS Catal.*, 2020, **10**, 11623–11633.
- 104 L. Falivene, Z. Cao, A. Petta, L. Serra, A. Poater, R. Oliva, V. Scarano and L. Cavallo, *Nat. Chem.*, 2019, **11**, 872–879.
- 105 J. K. Badenhoop and F. Weinhold, *J. Chem. Phys.*, 1997, **107**, 5422–5432.
- 106 M. Nishio, *Phys. Chem. Chem. Phys.*, 2011, **13**, 13873–13900.
- 107 R. Credendino, L. Falivene and L. Cavallo, *J. Am. Chem. Soc.*, 2012, **134**, 8127–8135.
- 108 I. Fernández, N. Lugan and G. Lavigne, *Organometallics*, 2012, **31**, 1155–1160.
- 109 M. Süßner and H. Plenio, *Chem. Commun.*, 2005, 5417–5419.
- 110 M. Álvarez-Moreno, C. de Graaf, N. López, F. Maseras, J. M. Poblet and C. Bo, *J. Chem. Inf. Model.*, 2015, **55**, 95–103.

